Observation of Landau-Zener dynamics in classical optical systems

D. Bouwmeester, N.H. Dekker, F.E. v. Dorsselaer, C.A. Schrama, P.M. Visser, and J.P. Woerdman
Huygens Laboratory, University of Leiden, P.O. Box 9504, 2300 RA Leiden, The Netherlands
(Received 15 March 1994; revised manuscript received 11 July 1994)

We report the observation of "tunneling" effects in a classical optical two-level system. In particular, we present experimental results for the optical implementations of the Landau-Zener model and of a hidden level-crossing model. The experimental results are in good agreement with theory for both the transition probability and the detailed time evolution of the wave function.

PACS number(s): 32.80.Bx, 33.80.Be

I. INTRODUCTION

Over the past few years optical resonators have been studied as model systems for quantum physics (see Ref. [1] for a review). Phenomena that are usually associated with the realm of quantum physics such as Rabi oscillations, Autler-Townes doublet splitting, Bloch-Siegert shifts, and multiphoton resonances have been demonstrated [2–4]. Generally, the experimental setup consisted of an optical cavity containing time-varying optical elements which drive the intracavity optical field. Almost all phenomena observed so far were (nearly) adiabatic in nature. Upon increasing the rate of change and the strength of the driving optical elements the onset of diabatic dynamics has been observed [3]. However, it was argued that the analogy with quantum physics would cease to hold if the rate of change or the strength of the optical elements would become sufficiently large [1,5]. Particular concerns were raised regarding the small lengths of the optical elements compared to the optical cavity length, and regarding the coupling to the various longitudinal modes of the optical cavity. Only recently was it understood that the correspondence between a two-level quantum system and a two-level optical system remains valid in the diabatic limit [6]. In this article we present experimental results showing both adiabatic and diabatic dynamics.

The most familiar level-crossing model for which diabatic dynamics is possible is the Landau-Zener (LZ) model [7,8]. In this model the diabatic, i.e., the unperturbed, energy levels cross linearly in time and the coupling is constant. The adiabatic energy levels form an avoided crossing and are coupled due to the time dependence of the adiabatic eigenstates. For strong time dependence and small energy separation of the adiabatic eigenstates, there is a large population transfer between these states. This phenomenon of Landau-Zener "tunneling" is usually associated with quantum mechanics. We report the observation of Landau-Zener transitions over the full dynamic range, i.e., from the adiabatic limit to the diabatic limit, in a classical optical two-level system.

Variations of the LZ model in which the diabatic energy levels do not cross but for which complex degeneracies of the adiabatic energy exist have recently been studied theoretically [9,10]. We will refer to such models as hidden-crossing models. In this article we present an optical implementation of a particular hidden-crossing model introduced by Fishman, Mullen, and Ben-Jacob [9]. We benefit from the macroscopic nature of the optical system which allows for a precise control of the energy-level structure, in contrast to atomic experiments where the relevant parameters are difficult to control. Furthermore, in atomic experiments it is impossible to measure directly the evolution of the populations, or of the atomic wave function, since the measurement always disturbs the wave function. In our optical experiment, however, the optical wave function can continuously be monitored without influencing its dynamics.

It is noteworthy that the introduction of Ref. [9] starts with the following statement: "The phenomenon of Zener-Landau tunneling, or nonadiabatic transitions, is a canonical example of a quantum-mechanical effect without a classical analog." Despite this statement we find experimentally good agreement with the theoretical work presented in Ref. [9]. The reason is that tunneling is a wave mechanical concept, valid for quantum *and* classical waves.

Our paper is organized as follows. The mathematical correspondence between the descriptions of an optical two-level system and a quantum-mechanical two-level system is presented in Sec. II. In Sec. III we present a brief theoretical review of two-level dynamics. In Sec. IV the experimental setup is described. The experimental results for the optical implementations of the LZ model and the hidden-crossing model are presented in Sec. V. Conclusions are drawn, and discussions are given in Sec. VI.

II. OPTICAL CAVITIES AND QUANTUM MECHANICS

The essential idea of the analogy between an optical cavity and quantum-mechanical system is that the optical field inside the cavity is mapped onto the quantum-mechanical wave function. Each optical resonance frequency provides an "energy level" for the optical field.

In this article we are particularly interested in two-level systems. The reduction to such systems is obtained by considering only two orthogonal polarizations of a single longitudinal mode of a Fabry-Pérot cavity. Experimentally, we use a frequency-stabilized injection laser which initially populates a single longitudinal mode in a well-defined polarization state. As soon as the optical system is prepared in the initial state the injection light is shut off. Subsequently, the optical elements inside the cavity are driven such that the polarization of the intracavity light will evolve approximately within the polarization manifold of the selected longitudinal mode. Specific driving of the optical elements results in an evolution of the polarization two-vector similar to the evolution of a quantum-mechanical state vector. Complications due to the finite speed of light and the presence of neighboring longitudinal modes are neglected; these are discussed in Ref. [6].

The energy degeneracy of the two orthogonal polarizations is lifted by an intracavity electro-optic modulator (EOM). An EOM consists of a crystal of which the birefringence is proportional to the voltage applied over it. To obtain a coupled two-level system we include a second EOM in the cavity, with its principal axes placed at 45° with respect to the axes of the first EOM. In the experiment a small fraction of the light propagating in, say, the positive z direction, leaks through one of the cavity mirrors thus providing the detection signal. The mathematical formalism employed to describe the slowly varying amplitudes of the two orthogonal polarizations at the position of the outcoupling mirror is the Jones-matrix formalism [11]. In this formalism each optical element is described by a 2×2 matrix. Multiplying these matrices for a closed optical path provides the round-trip matrix $M(t)$. We will neglect optical losses so that $M(t)$ is a unitary matrix. The experiments presented in this article are within the limit that $M(t+T) \approx M(t)$, where T is the round-trip time. This implies that $M(t)$ is approximately constant during a single round-trip time.

The evolution of the electric field envelope at the position of the outcoupling mirror is then obtained by

$$\vec{E}(t+T) = M(t)\vec{E}(t). \tag{1}$$

Here $\vec{E}(t)$ is given by

$$\vec{E}(t) = a_x(t)\hat{\vec{x}} + a_y(t)\hat{\vec{y}}, \tag{2}$$

where $a_x(t)$ and $a_y(t)$ change slowly compared to the optical frequency. THe two orthonormal basis states are indicated by $\hat{\vec{x}}$ and $\hat{\vec{y}}$.

For a round trip through the linear cavity used in our experiments, shown in Fig. 4 below, $M(t)$ is of the following form

$$\begin{aligned} M(t) &= B_2(t)B_1(t)B_1(t)B_2(t) \\ &= \begin{pmatrix} -i\sin\phi_1 + \cos\phi_1\cos\phi_2 & -i\cos\phi_1\sin\phi_2 \\ -i\cos\phi_1\sin\phi_2 & i\sin\phi_1 + \cos\phi_1\cos\phi_2 \end{pmatrix}, \end{aligned} \tag{3}$$

where the Jones matrices for EOM1 and EOM2 are given by

$$B_1(t) = \begin{pmatrix} e^{-i\phi_1/2} & 0 \\ 0 & e^{i\phi_1/2} \end{pmatrix}, \tag{4}$$

and

$$B_2(t) = \frac{1}{2}\begin{pmatrix} 1 & -1 \\ 1 & 1 \end{pmatrix}\begin{pmatrix} e^{-i\phi_2/2} & 0 \\ 0 & e^{i\phi_2/2} \end{pmatrix}\begin{pmatrix} 1 & 1 \\ -1 & 1 \end{pmatrix}. \tag{5}$$

The phase shifts ϕ_1 and ϕ_2 are proportional to the time-dependent voltages applied to EOM1 and EOM2, respectively.

In order to show the correspondence of the evolution of $\vec{E}(t)$, with the Schrödinger evolution of a quantum-mechanical wave function $|\psi(t)\rangle$ we integrate the Schrödinger equation over one round-trip time T,

$$|\psi(t+T)\rangle = U(t+T,t)|\psi(t)\rangle, \tag{6}$$

where

$$U(t+T,t) = \mathcal{T}\exp\left\{-\frac{i}{\hbar}\int_t^{t+T} H(t')\,dt'\right\}. \tag{7}$$

Time ordering indicated by $\mathcal{T}$ is necessary if $H(t)$ and $H(t+T)$ do not commute. However, we assume that $H(t+T) \approx H(t)$, corresponding to the assumption above that $M(t+T) \approx M(t)$. Therefore, Eq. (7) reduces to

$$U(t+T,t) \equiv U(t) = \exp\left\{-\frac{i}{\hbar}H(t)T\right\}. \tag{8}$$

If we include the factor $T/\hbar$ in the matrix elements of $H(t)$ and if we restrict ourselves to real symmetric matrices then Eq. (8) reads

$$\begin{aligned} U(t) &\equiv \exp\left\{-i\tilde{R}(t)\right\} \\ &= \exp\left\{-i\begin{pmatrix} \tilde{\phi}_1(t) & \tilde{\phi}_2(t) \\ \tilde{\phi}_2(t) & -\tilde{\phi}_1(t) \end{pmatrix}\right\}, \end{aligned} \tag{9}$$

where $\tilde{\phi}_1$ and $\tilde{\phi}_2$ represent phase shifts per round-trip time T.

The round-trip matrix $M(t)$ bears obvious resemblance to the Schrödinger propagator $U(t)$. In order to make the correspondence explicit we must express the round-trip matrix as an exponent of some Hermitian matrix R, $M(t) = \exp\{-iR(t)\}$. Since $M(t)$ is an unitary matrix there always exists a $R(t)$ that fulfills this requirement.

For $M(t)$ given by Eq. (3) $R(t)$ is of the following form:

$$R(t) = \frac{\varphi}{\sin\varphi}\begin{pmatrix} \sin\phi_1 & \cos\phi_1\sin\phi_2 \\ \cos\phi_1\sin\phi_2 & -\sin\phi_1 \end{pmatrix}, \tag{10}$$

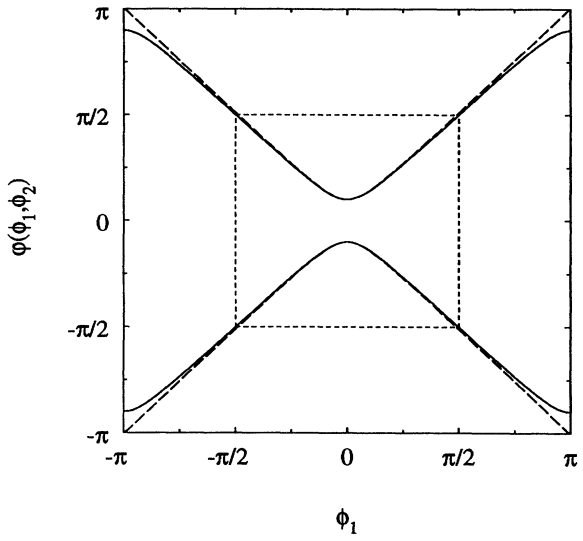

FIG. 1. The solid and dotted lines represent the eigenvalues φ of $R(t)$ and $\tilde{R}(t)$, respectively, as functions of ϕ_1 ($-\pi \leq \phi_1 \leq \pi$) for constant ϕ_2 ($\phi_2 = 0.1\pi$).

where $\varphi = \arccos(\cos\phi_1 \cos\phi_2)$.

We conclude that the optical system characterized by $R(t)$ corresponds to a quantum-mechanical system characterized by $\tilde{R}(t)$ if $R(t) \approx \tilde{R}(t)$. To examine whether or not this relation holds we identify ϕ_1 and ϕ_2 with $\tilde{\phi}_1$ and $\tilde{\phi}_2$, and plot in Fig. 1 the eigenvalues of $R(t)$ and $\tilde{R}(t)$ as functions of ϕ_1 for $\phi_2 = 0.1\pi$.

Comparing the eigenvalues of $R(t)$ and $\tilde{R}(t)$, and comparing the corresponding eigenstates, leads to the conclusion that $R(t) \approx \tilde{R}(t)$ if

$$-\frac{\pi}{2} \leq \phi_1 \leq \frac{\pi}{2}, \quad \text{and} \quad \phi_2 \ll 1. \tag{11}$$

These requirements are easily fulfilled in the experiments that we present in this article.

III. THEORY OF TWO-LEVEL DYNAMICS

In this section we briefly review the quantum-mechanical approach to two-level dynamics determined by real symmetric Hamiltonians.

A. The adiabatic representations

To obtain a good understanding of level dynamics it is useful to give a description in the adiabatic representation. The adiabatic basis at time t is formed by the two instantaneous eigenstates of $H(t)$, where $H(t)$ is given in the diabatic, i.e., the time-independent, representation. For real symmetric Hamiltonians $H(t)$ is of the form

$$H(t) = \begin{pmatrix} S(t) & V(t) \\ V(t) & -S(t) \end{pmatrix}. \tag{12}$$

The time-dependent adiabatic basis vectors are written as follows:

$$|\chi_1(t)\rangle \equiv \begin{pmatrix} \cos(\theta/2) \\ -\sin(\theta/2) \end{pmatrix}, \quad |\chi_2(t)\rangle \equiv \begin{pmatrix} \sin(\theta/2) \\ \cos(\theta/2) \end{pmatrix}, \tag{13}$$

where

$$\tan\theta = -\frac{V(t)}{S(t)}, \tag{14}$$

and

$$0 \leq \theta(t) \leq \pi. \tag{15}$$

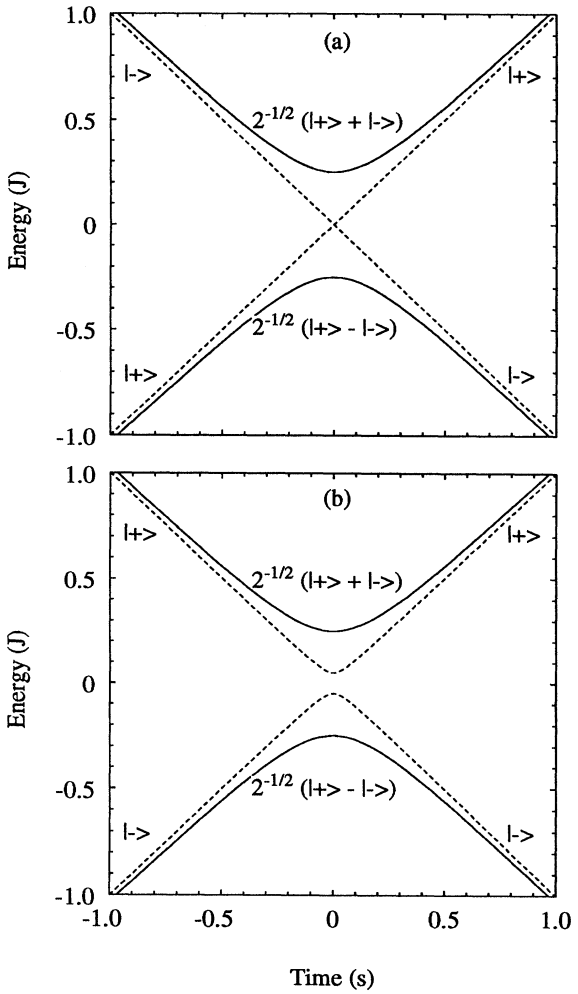

FIG. 2. (a) The solid curves represent the adiabatic energy levels of the Landau-Zener Hamiltonian, $H_{\rm LZ}(t)$, for $\alpha = 1.00$ J/s, and $\Delta = 0.25$ J. The dashed curves represent the diabatic ($\Delta = 0$) energy levels. (b) The solid curves represent the adiabatic energy levels of the Hamiltonian for the hidden-crossing model, $H_{|\rm LZ|}(t)$, for $\alpha = 1.00$ J/s, $\delta = 0.05$ J, and $\Delta' = 0.245$ J. The dashed curves represent the diabatic ($\Delta' = 0$) energy levels. Note that in (a) the diabatic energies cross at $t = 0$ whereas in (b) the diabatic energy levels form an avoided crossing at $t = 0$.

The adiabatic representation of the Hamiltonian, $\mathcal{H}$, is

$$\mathcal{H}(t) = \begin{pmatrix} -\epsilon(t) & -i\gamma(t) \\ i\gamma(t) & \epsilon(t) \end{pmatrix}, \tag{16}$$

where the energies of the adiabatic eigenstates are

$$\pm\epsilon(t) = \pm\sqrt{S^2(t) + V^2(t)}, \tag{17}$$

and the adiabatic coupling is

$$\gamma(t) = \frac{\dot{\theta}}{2} = \langle\chi_1|\dot{\chi}_2\rangle = \frac{V(t)\dot{S}(t) - \dot{V}(t)S(t)}{2[S^2(t) + V^2(t)]}. \tag{18}$$

For time derivatives the dot symbol is used. Note that the two adiabatic energy levels are coupled due to the rate of change of the adiabatic basis vectors.

B. The Landau-Zener model

The Landau-Zener model is characterized by a linear crossing in time of the diabatic energy levels, $S(t) = \alpha t$, and by a constant coupling, $V(t) = \Delta$. Hence in the diabatic representation the Landau-Zener Hamiltonian reads

$$H_{\mathrm{LZ}}(t) = \begin{pmatrix} \alpha t & \Delta \\ \Delta & -\alpha t \end{pmatrix}. \tag{19}$$

The solid and dotted curves in Fig. 2(a) show the adiabatic and diabatic energy curves of the Landau-Zener model, respectively.

The Landau-Zener model is one of the few models of two-level dynamics for which the Schrödinger equation is exactly solvable [12]. If at time $t = -\infty$ the system is prepared in the adiabatic state $|\chi_1(-\infty)\rangle = |+\rangle$ then the final transition probability P_f to the other adiabatic state $|\chi_2(+\infty)\rangle = |+\rangle$ is given by

$$P_f = \exp(-\pi/\Gamma), \tag{20}$$

where the so-called adiabaticity parameter Γ is given by

$$\Gamma = \hbar\alpha/\Delta^2. \tag{21}$$

In anticipation of the comparison of the experimental results with theory we introduce $\tilde{\alpha}$ and $\tilde{\Delta}$ as phase shifts per round-trip time T so that we may write

$$H_{\mathrm{LZ}}(t) = \frac{\hbar}{T}\tilde{R}_{\mathrm{LZ}}(t) = \frac{\hbar}{T}\begin{pmatrix} \tilde{\alpha}t & \tilde{\Delta} \\ \tilde{\Delta} & -\tilde{\alpha}t \end{pmatrix}, \tag{22}$$

and

$$\Gamma = \hbar\alpha/\Delta^2 = \tilde{\alpha}T/\tilde{\Delta}^2. \tag{23}$$

C. Hidden-crossing models

Variations of the LZ model in which the diabatic energy levels do not cross have recently been studied theoretically [9,10]. Although neither the adiabatic nor the diabatic energy levels cross in time there are nonzero transition probabilities. By analytical continuation of the adiabatic energy levels in the complex time or space plane there are in general points where the levels do cross [13]. Models for which the diabatic energy levels do not cross and for which complex degeneracies of the adiabatic energy levels exist are referred to as hidden-crossing models.

We have studied experimentally a particular hidden-crossing model for which the adiabatic energy levels are identical to the LZ levels as shown in Fig. 2(b). This model was introduced by Fishman, Mullen, and Ben-Jacob [9]: it is characterized by the following Hamiltonian

$$H_{|\mathrm{LZ}|}(t) = \begin{pmatrix} (\alpha^2t^2 + \delta^2)^{1/2} & \Delta' \\ \Delta' & -(\alpha^2t^2 + \delta^2)^{1/2} \end{pmatrix}. \tag{24}$$

For $\delta = 0$ this Hamiltonian reduces to

$$H_{|\mathrm{LZ}|}(t) = \begin{pmatrix} \alpha|t| & \Delta' \\ \Delta' & -\alpha|t| \end{pmatrix}, \tag{25}$$

hence we attached the notation |LZ| to this model. Although the adiabatic energy levels are the same in Figs. 2(a) and 2(b) (for $\delta^2 + \Delta'^2 = \Delta^2$), the transition probabilities are completely different for the two models. This emphasizes the fact that the coupling between the adiabatic energy levels is dominated by the time derivatives of the adiabatic energy eigenstates. In Fig. 3 the adiabatic coupling strength $\gamma(t)$ as given by Eq. (18) is plotted as a function of time for the LZ model (solid curve) and the |LZ| model (dashed curve).

Note that for the |LZ| model there are two domains, antisymmetric around $t = 0$, which significantly contribute

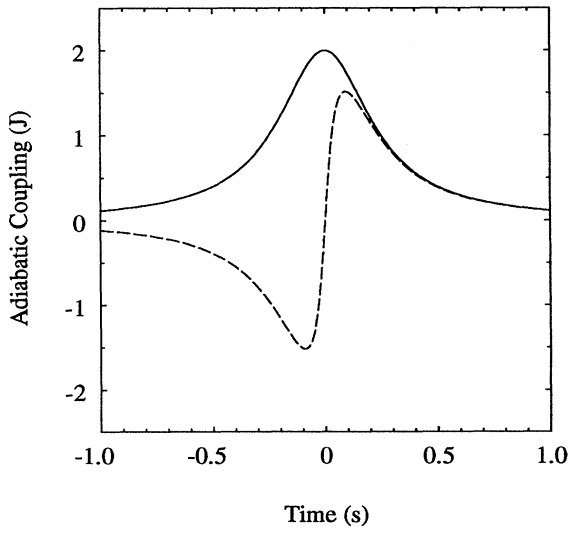

FIG. 3. Plot of the adiabatic coupling strength γ as function of time for the LZ model (solid curve, $\alpha = 1.00$ J/s, and $\Delta = 0.25$ J), and for the |LZ| model (dashed curve, $\alpha = 1.00$ J/s, $\delta = 0.05$ J, and $\Delta' = 0.245$ J).

to the transition probability. In the adiabatic limit and in the diabatic limit the state vector will evolve as indicated by the solid curve and dashed curve in Fig. 2(b), respectively. In the intermediate regime the combined effect of the two domains of adiabatic coupling give rise to population transfer. So far, analytical approximations are only known for the transition probabilities in the adiabatic and diabatic limit [9]. In the intermediate regime only numerical calculations have been reported [9]. The main feature of the |LZ| model is the $|t|$ time dependence, the precise value of δ is of minor importance. We will hereafter take $\delta = 0$. Again in anticipation of the comparison of the experimental results with theory we use $\tilde{\alpha}t \equiv \alpha t T/\hbar$, and $\tilde{\Delta}' \equiv \Delta' T/\hbar$.

IV. EXPERIMENTAL SETUP

In this section we discuss the experimental implementation of the Landau-Zener and the hidden-crossing models. Figure 4 shows the optical part of the experimental setup. The key elements are the two EOM's that are placed in a Fabry-Pérot cavity. The length of the cavity is 0.86 m and the mirrors, $M1$ and $M2$, have reflectances of 99.8%. The round-trip time T is $2L/c = 5.7$ ns. EOM1 is a low-voltage EOM ($\lambda/2$-voltage = 200 V) which is driven by the amplified output of an arbitrary-wave-form generator. The value of $\tilde{\alpha}(t)$ is proportional to the applied voltage. EOM2, placed with its axes at 45° with respect to those of EOM1, is a high-voltage EOM ($\lambda/2$ voltage = 4 kV). The parameter $\tilde{\Delta}$, proportional to the applied voltage over EOM2, is constant during each experimental run.

Injection light, provided by a single-mode frequency-stabilized 633 nm He-Ne laser, is linearly polarized along one of the axes of EOM1 and then coupled into the cavity through mirror $M1$. The cavity is made resonant with the injection light by slowly scanning the cavity length with a piezo element (PZT) mounted behind $M2$. When the cavity is scanned into resonance, detected by the photodiode APD1, the injection light is switched off by an acousto-optic modulator (AOM) permitting us to study the evolution of the intracavity light, without further injection. By using the first-order reflected beam from the AOM the injection light is switched off by removing the AOM voltage. The switching occurs within 10 ns since we focus the incident beam inside the AOM. Subsequently EOM1 is driven by the arbitrary-wave-form generator to create either the Landau-Zener or the hidden-crossing model. The constant voltage applied to EOM2 is changed to vary the adiabaticity parameter Γ ($\Gamma = \tilde{\alpha}T/\tilde{\Delta}^2$) [15].

To ensure that the light in the cavity has a lifetime sufficient for the experiment, a He-Ne discharge tube is inserted into the cavity to serve as a polarization-independent amplifier. To obtain polarization-independent amplification we mounted flat windows (double-sided antireflection coated at 633 nm) onto the capillary facets, instead of Brewster windows. We operate the optical cavity closely below laser threshold to avoid saturation of the gain medium which would introduce a polarization anisotropy. In this way the finesse is increased from 60 to 2500; this corresponds to a photon cavity lifetime of approximately 2 μs.

The light that leaks through $M2$ passes through a nonpolarizing beam splitter. One path permits us to detect the total light intensity, whereas the other path includes a polarizer and provides the detection signal for the intensity of the light polarized along the direction of the injection beam. Thus we can measure the intensity of, for instance, the x-polarization component of the light, which gives us information about the population transfer between the diabatic eigenstates. For detection we use two dc avalanche photo diodes (APD1 and APD2), with a bandwidth of 200 MHz. In order to enhance the signal to noise ratio, we average over 100 experimental runs taken within 10 s.

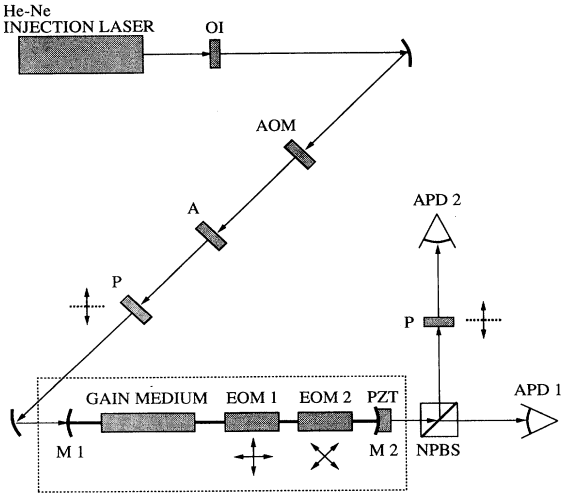

FIG. 4. Experimental setup. The acronyms used are OI for optical isolator, AOM for acousto-optic modulator, A for attenuator, P for polarizer, M for mirror, EOM for electro-optic modulator, PZT for piezo element, NPBS for nonpolarizing beam splitter, and APD for avalanche photo diode. The dotted line surrounds the Fabry-Pérot cavity.

V. EXPERIMENTAL RESULTS

A. The Landau-Zener model

Before proceeding to discuss the final results, we will illustrate some of the intermediate steps. Figure 5(a) depicts the result of a single-run Landau-Zener measurement. By comparing the signals of APD1 and APD2 we observe that before the transition occurs at time $t \approx 0.75$ μs the light is polarized along the x axis, i.e., in one adiabatic eigenstate only. The total intensity of the light undergoes an exponential decay because the optical system is operating slightly below laser threshold. After the transition light is present in both adiabatic eigenstates. Since the adiabatic eigenstates in the vicinity of the avoided crossing are superpositions of x- and y-polarized light a beat frequency is visible in the bottom trace of Fig. 5(a), i.e., in the intensity of the x polar-

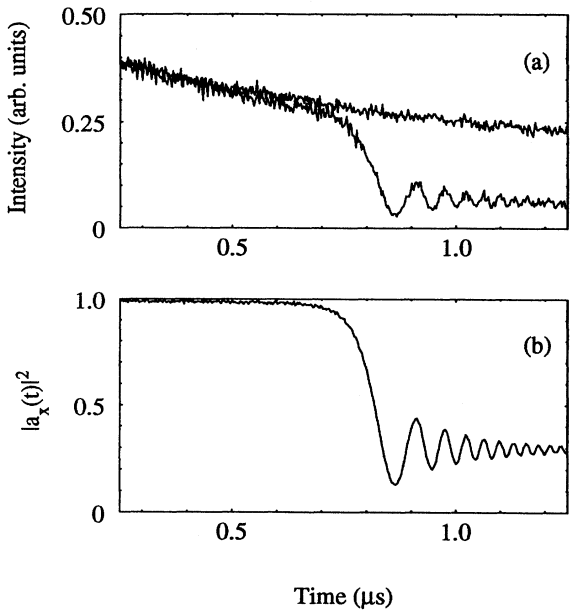

FIG. 5. Landau-Zener dynamics: (a) Signal from a single-run measurement, $\Gamma = 2.61$. The top trace is the total intensity as measured by APD1. The bottom trace is the intensity of the x component of the polarization measured by APD2. (b) Signal averaged over 100 runs and normalized, $\Gamma = 2.61$. The normalized intensity of the x polarization corresponds to $|a_x(t)|^2$.

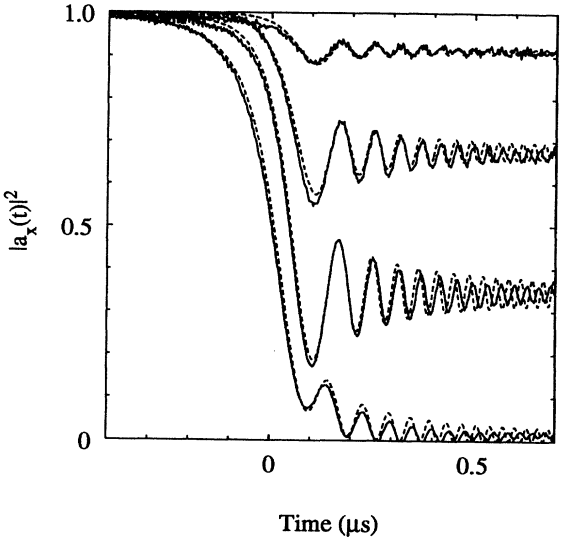

FIG. 6. Landau-Zener dynamics: comparison of experiment and theory for (top to bottom) $\Gamma = 34.8$, $\Gamma = 8.01$, $\Gamma = 2.93$, and $\Gamma = 0.71$. The solid traces show the experimental results and the dashed curves show the corresponding theoretical results.

ization. As time increases beyond the transition the frequency of the oscillation increases which indicates that the levels are being pulled further apart. Figure 5(b) shows the same dynamics, but now we have averaged over 100 runs and normalized the x-polarization signal by dividing by the total intensity. The normalized intensity of the x polarization corresponds to $|a_x(t)|^2$, where $a_x(t)$ is defined in Eq. (2). The graph shown in Fig. 5(b) is quite remarkable since it allows the verification of the Landau-Zener theory in all detail. Not only the final transition probability is measured but also the exact time evolution of the wave function.

In Fig. 6 we compare the experimental results with the theoretical predictions. The solid traces in Fig. 6 show optical Landau-Zener measurements for different values of Γ. In the experiments the $\tilde{\alpha}$ parameter was constant, $\tilde{\alpha} = (1.02 \pm 0.01) \times 10^6\ \mathrm{s}^{-1}$. The corresponding range of ϕ_1 during a single-run experiment of 2 μs is

$$-0.2\pi \leq \phi_1 \leq 0.2\pi\,. \tag{26}$$

The adiabaticity parameter Γ is varied by changing the $\tilde{\Delta}$ parameter. The maximum value of $\tilde{\Delta}$ used in the experiments corresponds to $\phi_2 = 0.1\pi$. The bottom trace shows the near-adiabatic regime in which the system follows the time-dependent adiabatic eigenstates; it proceeds from initial x- to final y-polarized light. As Γ is increased, the transition probability between the adiabatic eigenstates becomes larger and the final state contains x-polarized light as well. The top trace shows the near-diabatic regime, in which the light remains almost completely in the x-polarized state.

Without using any fit parameter the experimental data in Fig. 6 are in excellent agreement with the theoretical predictions (dashed curves).

There are only two minor differences between the experimental and theoretical results. First, the oscillation frequencies of the theoretical curves and the experimental traces do not exactly match. This deviation is, however, within the experimental inaccuracy of 1.5% in the determination of $\tilde{\alpha}$ and $\tilde{\Delta}$.

Second, in the experiments the oscillation amplitude decays slightly faster than the theory predicts. This indicates the loss of coherences between the two adiabatic eigenstates. A possible explanation is that spontaneous emitted light by the gain medium gives a small random contribution to the phase of the light inside the cavity. If the optical intensities decrease the relative influence of spontaneous emitted photons increases.

To quantify the agreement between theory and experiment, the theoretical predictions for the final transition probability P_f are plotted in Fig. 7 (solid curve) along with our experimental results (squares) as a function of Γ. The experimental values of P_f have been determined to an accuracy of 1% by taking the center values of the oscillations at the right-hand side of the traces in Fig. 6. Over the complete dynamical range we find agreement for the final transition probability to an accuracy of 2%.

B. The hidden-crossing model

The experimental results for the optical implementation of the |LZ| model are shown in Fig. 8. In this case

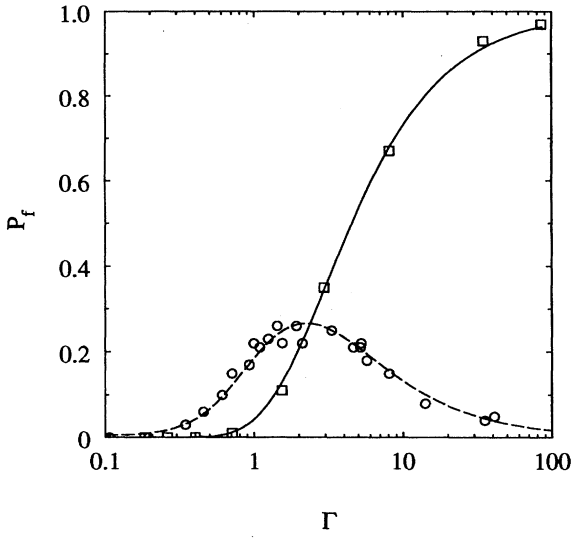

FIG. 7. Final transition probability P_f: The solid curve and the dashed curve show the theoretical predictions for the Landau-Zener model and the hidden-crossing model, respectively. The squares and the circles show the corresponding experimental data.

the parameter $\tilde{\alpha}(t)$, which determines the separation between the diabatic energy levels and which corresponds to the voltage applied over EOM1, is of the form $\tilde{\alpha}|t|$, where $\tilde{\alpha} = (6.02 \pm 0.05) \times 10^5$ s^{-1}. The parameter $\tilde{\Delta}'$, which is proportional to the voltage applied over EOM2, is again constant for each experimental run and is varied for different runs to change the adiabaticity parameter Γ.

In the adiabatic regime as shown in the top trace of Fig. 8, the light evolves from the x-polarized state to a superposition of the x- and y-polarized states, back to the x-polarized state. It corresponds to a zero transition probability between the adiabatic eigenstates. As Γ is increased (from top to bottom trace of Fig. 8), so does the transition probability, but only up to a certain value of Γ. Notice that the transition probability has a maximum around $\Gamma = 2.4$. This qualitative behavior is precisely as expected from the hidden-crossing model as reviewed in Sec. III. C. In Fig. 9 the experimental time traces and the theoretical curves for $\Gamma = 0.49$, and $\Gamma = 8.66$ are plotted [14].

Again good agreement between theory and experiment is obtained. To quantify the correspondence we plotted in Fig. 7 the experimental data (circles) obtained for the transition probability together with the theoretical predictions for P_f (dashed curve) as a function of Γ. Over the complete dynamical range we find agreement for the final transition probability to an accuracy of 3%.

VI. DISCUSSION AND CONCLUSIONS

We have experimentally demonstrated level-crossing dynamics, from the adiabatic to the diabatic regime, in classical optical systems. Despite the presence of additional optical levels (i.e., longitudinal modes) surrounding the two optical levels under study we find good agreement between optical experiments and theory, developed for quantum-mechanical systems. We have presented a direct experimental verification of the detailed time evolution of the wave function upon passing either an avoided crossing or a hidden crossing. The results for the two types of crossings show that the correspondence between optical systems and quantum systems remains valid within the diabatic limit. In addition, the good agreement between theory and experiment shows that the influence of retardation effects remains negligible on the time scales used in our experiments [6].

One clear difference between the quantum-mechanical wave function and the optical wave function is of course the influence of a measurement. Whereas in quantum mechanics the measurement destroys the phase information due to coupling to the macroscopic world, this so-

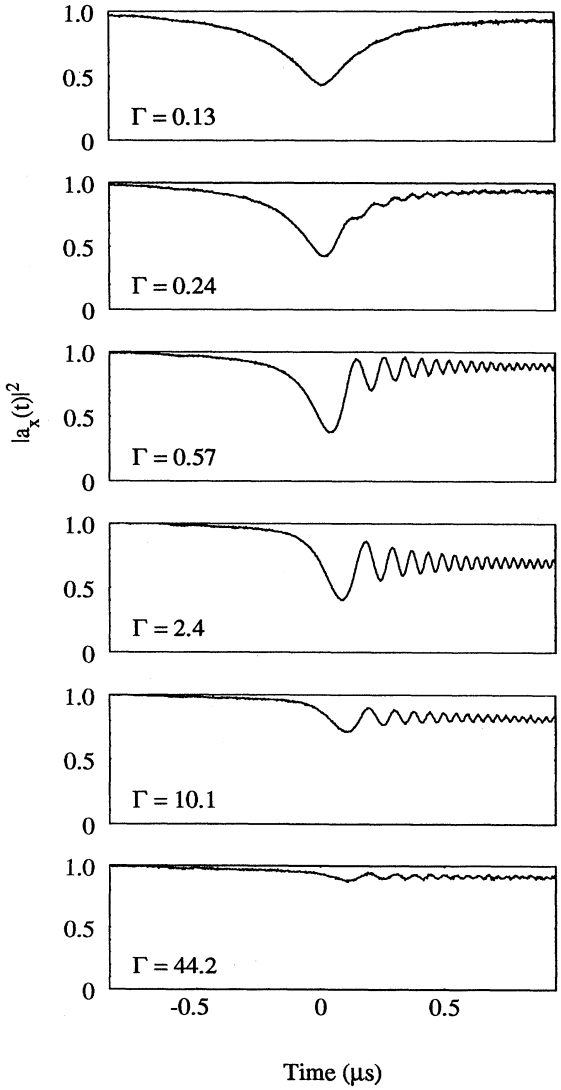

FIG. 8. |LZ| dynamics: normalized, averaged experimental data for different values of the adiabaticity parameter Γ.

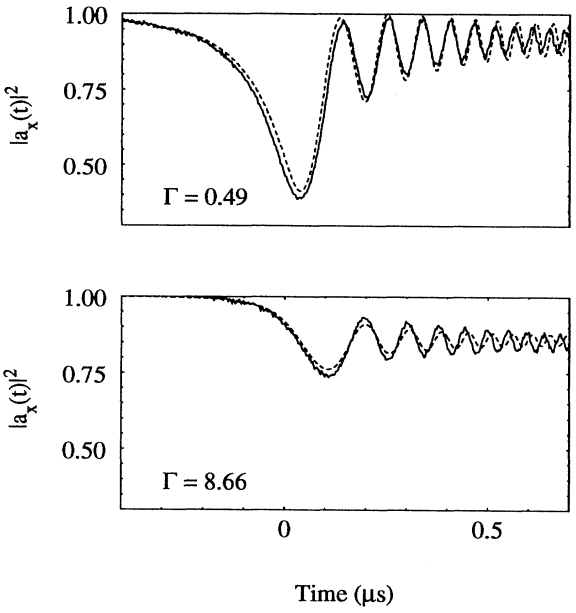

FIG. 9. |LZ| dynamics: comparison of experiment and theory for $\Gamma = 0.49$, and $\Gamma = 8.66$. The solid traces show the experimental results and the dashed curves show the corresponding theoretical results.

called collapse of the wave function is not present during the optical measurement. The fact that photons are bosons allows that the optical levels can be filled by many identical photons. We profitted from this boson character by including a light-amplifier tube which "clones" photons to replace those escaping from the cavity. Since the precise time evolution of the optical wave function is measurable, it is possible to examine histories of adiabatic "quantum" transitions in optical systems. This topic, which led Berry and Lim to the introduction of the superadiabatic basis [17–19], will be the subject of future experiments.

For the description of quantum-mechanical systems the appearance of $\hbar$ is usually believed to be a fundamental feature. In the description of the dynamics inside optical cavities all frequencies can be related to energies by the well-known relation $E = \hbar\omega$. Since in the description of the dynamics inside any two-level system only the relative differences between the energy or frequency levels is relevant, $\hbar$ becomes a superfluous constant. We have not set $\hbar = 1$ for this article; instead $\hbar$ simply vanishes from the equation of motion since all energies are related to frequencies.

Our experiments were limited to a finite time interval since the optical level structure deviates from the Landau-Zener level structure for $|t| \gg 0$. It is not necessary to interpret this deviation as a shortcoming of the optical system; rather it emphasizes the unphysical character of the Landau-Zener model for $t \to \pm\infty$. Variations on the Landau-Zener model have been introduced which are not beset by unphysical features for $t \to \pm\infty$ [16]. A detailed study of such models is within reach of optical experiments; however, this is outside the scope of the present article.

In this paper we have restricted ourselves to two-level systems with real Hamiltonians. Two-level models characterized by complex Hamiltonians offer new possibilities. Berry has pointed out that certain complex Hermitian Hamiltonians give rise to geometric amplitude factors [20]. It is possible, in principle, to generate such Hamiltonians in our setup. Experimental efforts are currently underway to observe the geometric amplitude factors in these optical systems.

ACKNOWLEDGMENTS

This work is part of the research program of the Foundation for Fundamental Research on Matter (FOM) and was made possible by the financial support from the Netherlands Organization for Scientific Research (NWO).

[1] R.J.C. Spreeuw and J.P. Woerdman, in *Progress in Optics*, edited by E. Wolf (North-Holland, Amsterdam, 1993), Vol. 31, pp. 263–319.
[2] R.J.C. Spreeuw, J.P. Woerdman, and D. Lenstra, Phys. Rev. Lett. **61**, 318 (1988).
[3] R.J.C. Spreeuw, N.J. van Druten, M.W. Beijersbergen, E.R. Eliel, and J.P. Woerdman, Phys. Rev. Lett. **65**, 2642 (1990).
[4] M.W. Beijersbergen, R.J.C. Spreeuw, L. Allen, and J.P. Woerdman, Phys. Rev. A **45**, 1810 (1992).
[5] R.J.C. Spreeuw (private communications).
[6] C.A. Schrama, D. Bouwmeester, G. Nienhuis, and J.P. Woerdman, preceding paper, Phys. Rev. A **51**, 641 (1995).
[7] L.D. Landau, Phys. Z. Sowjetunion **2**, 46 (1932).
[8] C. Zener, Proc. R. Soc. London Ser. A **137**, 696 (1932).
[9] S. Fishman, K. Mullen, and E. Ben-Jacob, Phys. Rev. A **42**, 5181 (1990).
[10] K.-A. Suominen, Opt. Commun. **93**, 126 (1992).
[11] R. Clark Jones, J. Opt. Soc. Am. **31**, 488 (1941).
[12] B.W. Shore, *The Theory of Coherent Atomic Excitations* (Wiley, New York, 1990), Vol. 1.
[13] J.P. Davis and P. Pechukas, J. Chem. Phys. **64**, 3129 (1976).
[14] Simulations for $P_{|\mathrm{LZ}|}$ were also presented in Ref. [9]. Since the simulations do not start at $t = -\infty$ the initial adiabatic eigenstates are not completely identical to the diabatic eigenstates. As initial state of the simulations in Ref. [9] one of the diabatic eigenstates was chosen. This corresponds to initially populating both the adiabatic eigenstates and thus to oscillations before the hidden crossing. In our simulations the initial state is an adiabatic eigenstate. Therefore, our simulations are free from spurious oscillations for $t < 0$.
[15] In the literature on Landau-Zener dynamics it is common to vary the parameter α. We choose to vary the parame-

ter Δ instead; this results in an equal time span for each experimental run.
[16] K.-A. Suominen and B.M. Garraway, Phys. Rev. A **45**, 374 (1992).
[17] M.V. Berry, Proc. R. Soc. London A **429**, 61 (1990).
[18] R. Lim and M.V. Berry, J. Phys. A **24**, 3255 (1991).
[19] M.V. Berry and R. Lim, J. Phys. A **26**, 4737 (1993).
[20] M.V. Berry, Proc. R. Soc. London Ser. A **430**, 405 (1990).